2-D Joint Inversion of Semi-Airborne CSEM and LOTEM Data in Eastern Thuringia, Germany

Ji Cai[1], Pritam Yogeshwar[1], Wiebke Mörbe[1], Maria Smirnova[1,2], Amir Haroon[3], Michael Becken[2] and Bülent Tezkan[1]

1. Institute of Geophysics and Meteorology, University of Cologne, Cologne, Germany
2. WWU Münster, Institute of Geophysics, Münster, Germany
3. GEOMAR Helmholtz Centre for Ocean Research, Kiel, Germany

Abstract

Various electromagnetic (EM) techniques have been developed for exploring natural resources. The novel frequency-domain semi-airborne controlled source electromagnetic (semi-AEM) method takes advantages of both ground and airborne techniques. It combines ground-based high-power electrical dipole sources with large scale and spatially densely covered magnetic fields measured via airborne receivers. The method can survey the subsurface down to approximately 1000 m and is particularly sensitive towards conductive bodies (e.g., mineralized bodies) in a more resistive host environment. However, the signal-to-noise ratio of semi-AEM is lower than that of ground-based methods such as long-offset transient electromagnetics (LOTEM), mainly due to the limited stacking time and motion induced noise. As a result, the semi-AEM often has reduced depth of investigation in comparison to LOTEM. One solution to overcome these flaws is to analyse and interpret semi-AEM data together with information from other EM methods using a joint inversion. Since our study shows that LOTEM and semi-AEM data have complementary subsurface resolution capabilities, we present a 2-D joint inversion algorithm to simultaneously interpret frequency-domain semi-AEM data and transient electric fields using extended dipole sources. The algorithm has been applied to the field data acquired in a former mining area in eastern Thuringia, Germany. The 2-D joint inversion combines the complementary information and provides a meaningful 2-D resistivity model. Nevertheless, obvious discrepancies appear between the individual and joint inversion results. Consequent synthetic modelling studies illustrate that the discrepancies occur because of i) differences in lateral and depth resolution

between the semi-AEM and LOTEM data caused by different measuring configurations, ii) different measured EM components, and iii) differences in the error weighting of the individual datasets. Additionally, our synthetic study suggests that more flexible land-based configurations with sparse receiver locations are possible in combination with semi-AEM without a significant loss of target resolution, which is promising for accelerating data acquisition and for survey planning and logistics, particularly when measuring in inaccessible areas.

Keywords: Controlled source electromagnetics (CSEM); Non-linear electromagnetics; Joint inversion

1 Introduction

Electromagnetic (EM) methods are applied to differentiate between resistivity variations of natural resources and their host rock environment. They are efficient tools for resource explorations, e.g. mineral detection (e.g., Mörbe et al., 2020), ground water investigation (e.g., Haroon et al., 2018b), hydrocarbon (e.g., Schwalenberg et al., 2017) and geothermal prospection (e.g., Commer et al., 2005). Recently, a novel semi-airborne controlled source electromagnetic (semi-AEM) system operating in frequency-domain has been developed and tested in the frame of the DESMEX (Deep Electromagnetic Sounding for Mineral Exploration) project (Becken et al., 2020; Smirnova et al., 2019). This DESMEX system aims to acquire dense CSEM data at relatively high survey speed (120 km/h) with an exploration depth of approximately 1 km. Compared to typical airborne EM systems with both transmitter (Tx) and receivers (Rx) installed on aircrafts, semi-AEM combines an increased penetration depth with dense spatial data coverage by using grounded high-power sources (e.g., Mogi et al., 2009; Mogi et al., 1998). However, a disadvantage compared to ground-based surveys is the reduced data quality due to motion-induced noises. Furthermore, due to the aircraft moving during the acquisition, there is no sufficient recording time for quality statistical estimates. Additionally, no electric field data can be obtained using semi-AEM, which can restrict the resolution of resistivity in certain geological settings.

CSEM techniques are often categorized into time- and frequency-domains methods, depending on the domain in which the data are interpreted. Ground-based time-domain CSEM measurements utilizing large offsets between the horizontal electric dipole (HED) and various electric and magnetic field receivers are commonly referred to as long-offset transient electromagnetic (LOTEM) measurements. The LOTEM method has been widely used for several decades, especially in the context of mineral exploration (cf. Strack, 1992). In a typical LOTEM survey, a large HED transmitter antenna of 1-2 km is utilized to inject a square-wave current signal with an amplitude of several tens amperes into the earth (Haroon et al., 2015), causing both inductive and galvanic effects (Kaufman & Keller, 1983). At various receiver sites separated 500 m up to several kilometres from the source, horizontal electric field components and magnetic fields are measured. Depending on the offset, noise sources and resistivity structure, LOTEM technique can be used to investigate the subsurface down to several kilometres (Mörbe, 2020; Haroon et al., 2015).

LOTEM can provide valuable complementary information to semi-AEM data to improve resolution. A combined interpretation of both techniques requires a joint-inversion approach. The merits of joint inversion were proposed by Vozoff & Jupp (1975) and further advanced in the following decades (e.g., Peng et al., 2021; Wang et al., 2019; Meqbel & Ritter, 2015; Commer & Newman, 2009; Meju, 1996). The EM inverse problem is ill-posed and, therefore, it is challenging to obtain geologically meaningful subsurface resistivity models that fit the observed data. Due to data errors, limited data coverage, and limited resolution, the EM inversion usually suffers from non-uniqueness, i.e., the data can fit into a number of different resistivity models (e.g., Cai et al., 2018; Gehrmann et al., 2016; Moghadas et al., 2015). Thus, some parameters in the derived resistivity models cannot be uniquely determined, and some artificial structures can appear in the inversion results. In this case, the joint inversion of several geophysical datasets can contribute to reducing model parameter uncertainties (Meqbel & Ritter, 2015). By jointly inverting the data of different geophysical methods, more independent information is considered, and results in a stronger constraint of the model parameters. The joint inversion can be applied not only to EM and electrical methods that are sensitive to electrical resistivity but also to other geophysical techniques such as seismic and gravity methods (e.g., Wagner et al., 2019; Moorkamp et al., 2011).

Based on extracting the different resolution characteristics of semi-AEM and LOTEM data, we intend to optimize mineral exploration surveys via the joint inversion of these two EM methods. In a large-scale mineral exploration survey conducted in the DESMEX frame in eastern Thuringia, Germany (Liu et al., 2020; Mörbe et al., 2020; Steuer et al., 2020; Smirnova et al., 2019), one 8.5 km long LOTEM profile was measured along one of the semi-AEM flight lines. Many other geophysical experiments were also conducted during the DESMEX survey. Steuer et al. (2020) present an integrated overview of the results and compare the models derived from various methods. In general, the 2-D resistivity models agreed well with respect to the main structures. However, some discrepancies in subsurface resistivity distributions were not negligible. Due to the complexity of the survey area, several factors could cause these discrepancies, e.g., multi-dimensional effects, induced polarization (IP) or anisotropy. Furthermore, discrepancies could have also occurred due to the different resolution properties of each method. Understanding the causes of these discrepancies is important in optimizing the final interpretation and therefore it is one of the main motivations of this study.

Specifically, this study focuses on the resolution characteristics when combining semi-AEM and LOTEM data to: (1) investigating the possible factors leading to the discrepancies between the LOTEM and semi-AEM individual inversion results in the DESMEX experiments; (2) implementing, verifying and applying a 2-D joint inversion approach for frequency-domain and time-domain data, and (3) evaluating the advantages and deficiencies of joint inversion in elaborate sensitivity studies. We first present a brief theoretical background, including the implementation of the 2-D joint inversion for frequency- and time-domain data, as well as the concepts and measuring systems of semi-AEM and LOTEM. Next, we describe synthetic modelling studies to evaluate the performance of the adapted 2-D joint inversion algorithm using MARE2DEM (Key, 2016) and apply it to field data. Subsequently, we investigate the robustness of the derived joint inversion models through further synthetic studies to understand the resolution characteristics of each method and try to analyse the causes of the discrepancies between field data individual and joint inversion results. Finally, since ground-based LOTEM is cumbersome, we present a synthetic study aiming at optimizing data acquisition workflow for future mineral exploration surveys using semi-AEM and LOTEM.

2 Experiment design

During the DESMEX project, two field experiments were conducted in 2016 (Mörbe et al., 2021) and 2017 in eastern Thuringia, Germany. The main objective of the two experiments was to test the newly developed semi-AEM system. Additionally, various complementary geophysical surveys were performed to validate the resulting semi-AEM resistivity models. Figure 1 displays the semi-AEM and the LOTEM surveys conducted on a NW-SE transect.

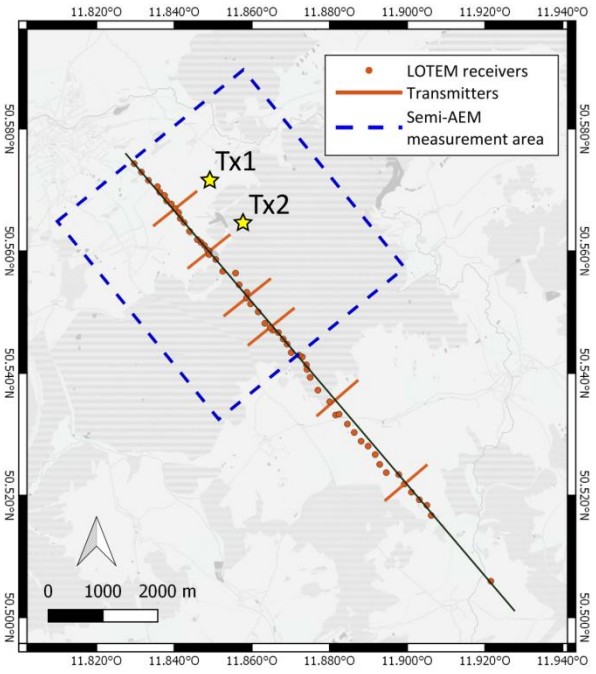

Figure 1. Location of the semi-AEM measurement area (modified based on Smirnova et al., 2019) and LOTEM measuring configurations (modified based on Mörbe et al., 2020) near Schleiz in eastern Thuringia, Germany in 2016 and 2017. The orange solid lines mark the transmitter positions; the two transmitters Tx1 and Tx2, highlighted by stars, were utilized for both semi-AEM and LOTEM measurements. Orange dots indicate the positions of the LOTEM receivers. The region marked by dashed blue lines is the area covered by semi-AEM flight lines.

2.1 LOTEM survey

In total, 6 transmitters and 52 receiver stations were deployed along an 8.5 km-long profile (Figure 1) using a broadside transmitter-receiver configuration. The length of the transmitter antenna was about 1 km and the

current amplitude was approximately 24 A. For this survey, we rotate the coordinate system so that the transmitter wire is regarded as x-directional. By utilizing multiple transmitter-receiver combinations we obtain a total of 170 Ex-component sites that were measured with electric dipoles between 40 and 60 m in length. Note that the LOTEM data mentioned in this paper are hereafter referred to as the Ex-components. After the processing in the time-domain (Mörbe et al., 2020), the LOTEM data were current normalized step-on signals with a time range between around 10^{-4} to 1 s. The processed data show standard deviations generally smaller than 1%. To account for systematic errors due to e.g., geometrical errors during setup, the data errors of LOTEM electric fields were evaluated by Mörbe (2020) and defined at 2%. Hence, a 2% Gaussian noise is always added to the synthetic LOTEM modelling presented hereafter.

2.2 Semi-AEM survey

The semi-AEM measurement area (Figure 1) from 2016 (NW-SE direction) is shorter than that of the LOTEM profile. Two LOTEM transmitters (Tx1 and Tx2, marked by yellow stars in Figure 1) were also employed during the semi-AEM flights. The magnetic sensor in the birds measured the magnetic fields at an altitude of roughly 50 meters, with a speed of 120 km/h. The gaps in data coverage over the vicinities of source positions can be filled in by the data from the other transmitter. The recorded magnetic fields were subsequently processed in the frequency-domain (Smirnova et al., 2019), resulting in CSEM transfer functions (T_z) between the vertical component of the magnetic field and the current. Where $\boldsymbol{B}(f) = \boldsymbol{T}(f)\boldsymbol{I}(f)$, $\boldsymbol{B}(f)$ denotes the observed magnetic flux densities and the $\boldsymbol{I}(f)$ indicates the injection currents (Becken et al., 2020). Time series were separated into 5 s time windows for calculating the T_z at certain locations, overlapping by 2.5 s. Along the LOTEM profile shown in Figure 1, semi-AEM data were acquired at around 30 receiver positions. Due to the moving receivers and the limited 5 s spatial averaging window length, the corresponding data errors derived from the standard deviations of the stacked semi-AEM data were higher than those of the LOTEM measurements. Moreover, the errors decrease with increasing frequency, ranging from 20% to 1% (Smirnova et al., 2019) for 10 Hz to 1000 Hz, respectively. For large offsets (> 2000 m), the signal-to-noise ratio reduced substantially, limiting the depth of investigation. For

simplification, the error estimations of semi-AEM data (both real and imaginary parts) are assumed to be 5% in the consequent synthetic modelling. The following table summarises the parameters of the measurement configurations for the two EM methods. Note that, the semi-AEM data includes only the transfer function of the vertical magnetic field in the frequency-domain and the LOTEM data consider only the current normalized Ex step-on transients. Thus, the transmitter current is always set as 1 A in the synthetic and inverse modelling.

Table 1. The considered measurement configurations of LOTEM and semi-AEM EM.

Method	LOTEM	semi-AEM
Domain	Time	Frequency
Component	Ex (Step-on)	$Re(T_z)\&Im(T_z)$
Tx position	Land	Land
Rx position	Land	Air
Tx-Rx separation	500 to 4000m	500 to 2000m

3 Implementation of a 2-D joint inversion for frequency- and time-domain data

The objective of the joint inversion in this paper is to find a common resistivity model that fits all the considered datasets from various EM methods. Therefore, the joint data vector (**d**), the forward operator (**F**), and the Jacobian matrix (**J**) represent a combination of each method, in our case LOTEM and semi-AEM:

$$\boldsymbol{d} \quad \left[\quad\right]; \quad \left[\quad\right]; \quad \left[\quad\right]; \tag{1}$$

The free model parameters or unknowns remained the same as those for inverting one single dataset. The Jacobian matrices are error weighted. Since no additional weighting scheme was implemented, there is no trade-off parameter or matrix between $\boldsymbol{J}_{LOTEM}$ and $\boldsymbol{J}_{Semi-AEM}$.

The 1-D joint inversion algorithm for LOTEM and semi-AEM data has been successfully developed and tested with synthetic data (Cai, 2020). As indicated by 1-D synthetic modelling studies presented in Figure A 1,

resolution differences between the two methods are observable due to the physical characteristics of the measured components (Ex versus Bz) and different error estimates. The combination of two methods with different resolutions provides the constraint on the equivalence domain, which is the fundamental advantage of the proposed joint inversion.

However, compared to the 1-D single method inversions, the 1-D joint inversion is more susceptible to inversion artifacts caused by multi-dimensional resistivity structures (see Figure A 2). Due to the multi-dimensional subsurface of this measurement area and the absence of an efficient 3-D time-domain inversion, a 2-D joint inversion algorithm is employed to interpret the LOTEM and semi-AEM data collected along the profile. Based on the original MARE2DEM presented by Key (2016) and its updated version that allows for the computation of time-domain signals (Haroon et al., 2018a), we have further adapted MARE2DEM to account for 2-D joint inversion of time- and frequency-domain data, which was not feasible in the previous code packages of MARE2DEM. MARE2DEM already supports joint inversion of magnetotelluric and CSEM data, which is thus a prerequisite to support the inclusion of the time-domain inversion in the adapted MARE2DEM algorithm. The corresponding finite-element details or fundamental theories are presented by Key (2016). More details about the unstructured triangle meshes, the adaptive refinement system, and the parallel implementations, are described in Li & Key (2007) and Key & Ovall (2011).

The semi-AEM concept is similar to the standard ground-based frequency-domain CSEM except that the receivers are positioned in the air (Smirnova et al., 2019). For all simulations, we assign the air layer a resistivity of 10^6 Ωm. By setting the receiver positions in the air layer and selecting the proper wavenumbers in MARE2DEM, accurate semi-AEM data can be achieved for the required frequencies. Specifically, we use 110 wavenumbers ranging from 10^{-4} to 10^6 to accurately compute real and imaginary parts of the T_z component from 10 Hz to 1000 Hz.

For simplicity, the general modelling for the frequency-domain data is referred to as the semi-AEM modelling, and the time-domain modelling as the LOTEM modelling. The concise workflow of our

MARE2DEM modifications is presented in

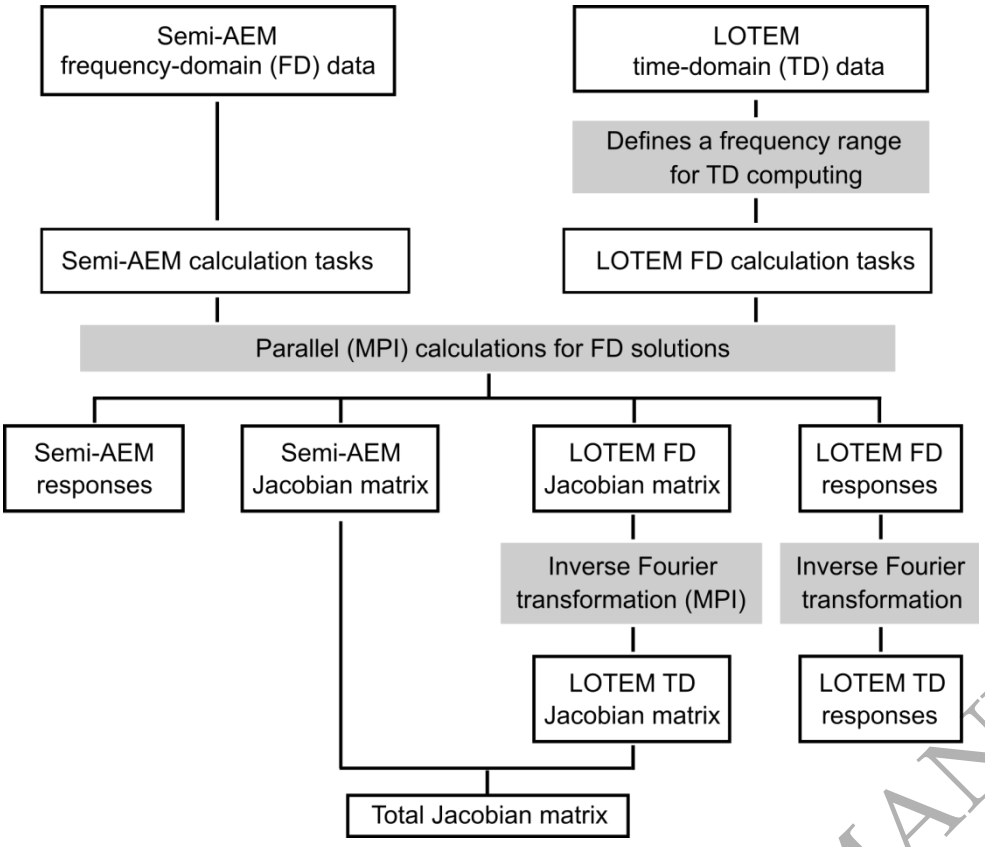

Figure 2. The semi-AEM solution and Jacobian matrix can be calculated using the original code developed by Key (2016). The Jacobian matrix is calculated by using adjoint reciprocity approach based on logarithmically transformed model parameters (Key, 2016). This part of computation is conducted by a Message Passing Interface (MPI) parallel algorithm, which divides the modelling task into smaller subtasks parallelizing the frequencies, transmitters, receivers and wavenumbers. The results computed by these parallel computations are subsequently gathered and integrated into the final frequency-domain solution and Jacobian matrix.

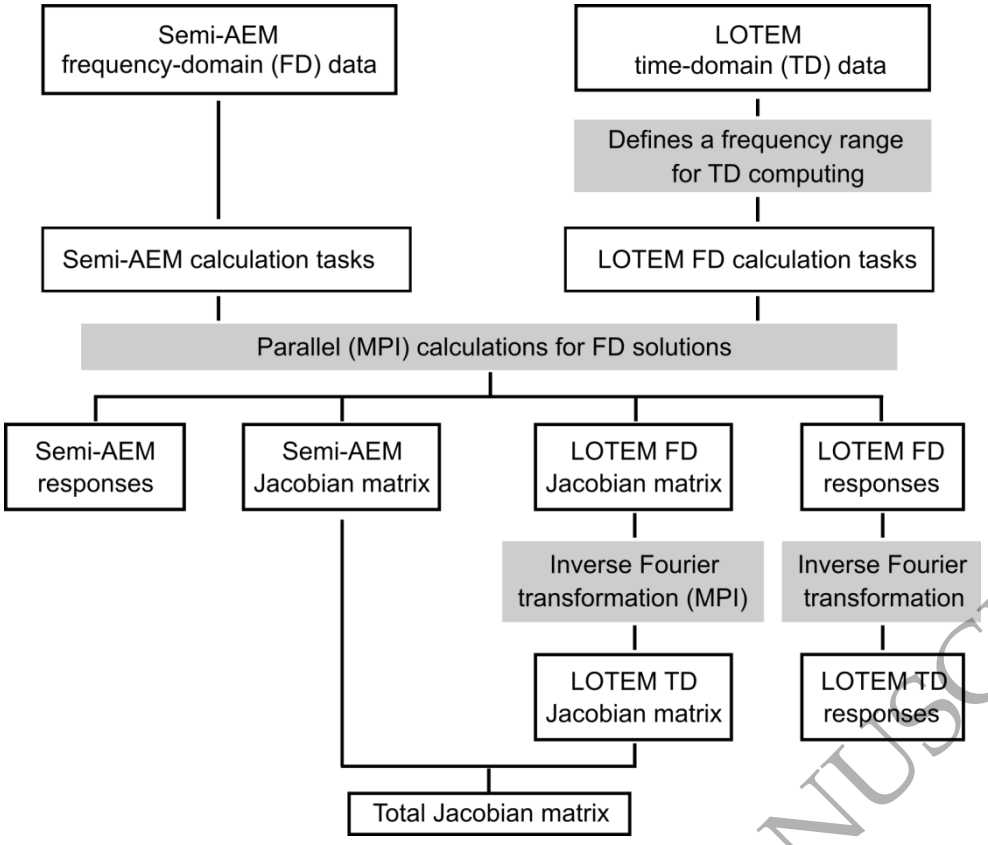

Figure 2. Workflow for realizing the joint inversion of semi-AEM and LOTEM data in MARE2DEM.

Haroon et al. (2018a) implemented the time-domain solutions into MARE2DEM by transforming frequency-domain solutions into the time-domain using the inverse Fourier Transformation (Anderson, 1982). For the time-domain solution, the Jacobian matrix is first computed in the frequency-domain and then transferred into the time-domain using parallel MPI computations but did not allow for simultaneous modelling of frequency- and time-domain data (Haroon et al., 2018a). Here, we updated the data module of MARE2DEM to account for both frequency- and time-domain data. Thus, the input information of both EM methods can be broadcasted and loaded simultaneously, and their sub-tasks can be computed in parallel. After the LOTEM Jacobian matrix is calculated via the inverse Fourier Transformation based on the required frequency-domain solutions, it can be combined with the semi-AEM Jacobian matrix (e.g., equation 1) and used to update the model.

4 2-D joint inversion

4.1 2-D synthetic study

We use synthetic forward and inverse modelling studies to analyse the resolution characteristics of semi-AEM and LOTEM data. We consider the canonical 2-D model shown in Figure 3a. A conductive layer (10 Ωm) with a thickness of 100 m is buried at a depth of 250 m in a more resistive host environment (300 Ωm). In the basement region (at 650 m depth), a lateral resistivity contrast is set at profile position of 0 m. The basement layer has a resistivity of 50 Ωm on the left side and 1000 Ωm on the right side.

In this modelling example, the horizontal positions of the receivers are consistent for semi-AEM and LOTEM measurements, and therefore the resolution divergence caused by different coverage of measuring configurations are excluded. LOTEM receivers are located on the earth's surface, whereas semi-AEM receivers are located at an altitude of 40 m. Synthetic data were calculated for two transmitters marked by circles in Figure 3a to d. Semi-AEM and LOTEM data were calculated for 21 frequencies ranging from 10 Hz to 1000 Hz, and for 24 time points ranging from 0.0005 s to 0.4 s, respectively. The LOTEM solutions were computed using 10 frequencies per decade (Haroon et al., 2018a) ranging from 2×10^{-5} to 4×10^{5} Hz. For the inversions, the ratio of the roughness between the horizontal and vertical directions is always set to 3. The starting value of the Lagrange parameter is always set to 10^5, and then a minimum search for lambda is performed within a fast Occam approach (Key, 2016). For the inversion studies, a misfit χ for evaluating the fit between calculated data $f_i(m)$ and observed (synthetic) data d_i is defined by,

$$\sqrt{-\sum \frac{(\ _i(m)-\ _i)^2}{(\Delta d_i)^2}} \quad , \tag{2}$$

where N is the number of the data points and Δd_i is the data error in the ith datum. The convergence of a joint inversion is usually evaluated by the total data misfit considering all the datasets. As stated earlier, error estimations are 2% for LOTEM and 5% for semi-AEM. To simulate realistic field conditions, the data was perturbed with Gaussian noise using the same values as above. The starting model is a 500 Ωm half space. Outside the inversion region which includes free parameters, the entire model domain is extended to

$\pm 10^5$ m in both horizontal and vertical direction in order to fit the Dirichlet boundary conditions. Figure 3b displays the 2-D inversion result for semi-AEM transfer functions of vertical magnetic field only; Figure 3c shows only results for LOTEM electric field data; and Figure 3d is the joint inversion results of both datasets. All three inversion models displayed in Figure 3b to d achieve a χ = 1.01.

The solo semi-AEM inversion (Figure 3b) clearly detects the upper and two horizontal boundaries of the shallow conductor. In comparison, the solo LOTEM inversion (Figure 3c) is less effective in detecting the geometry of the shallow conductor. In the joint inversion result of both datasets (Figure 3d), both the shallow conductive layer and the lateral resistivity contrast of the basement layer are better resolved. The latter is an obvious advantage of the joint inversion compared to the single semi-AEM and LOTEM inversion models. The joint inversion can detect the resistive basement on the right side of the model, with a clear representation of its depth, lateral extent, and a resistivity value of 1000 Ωm. The boundary of the conductive basement is not resolved as well as that of the resistive basement in the joint inversion model. Yet, it is depicted more clearly than in the individual inversions.

Overall, the synthetic modelling study indicates that joint inversion achieves a better estimate of the basement resistivity structure compared to the individual inversions of LOTEM and semi-AEM data. To further visualize sensitivity differences between the methods, cumulative sensitivities computed after Schwalenberg et al. (2002) in equation 3 are displayed by white contours.

$$-\sum_i^N \left\| - \frac{}{_i(m)} \right\|, \tag{3}$$

Here, *N* indicates the total number of data, and Δ_j denotes the area or size of the j^{th} grid element. According to equation 3, the larger sensitivity values indicate the stronger effects on the data caused by the resistivity variation of grid elements, which is the necessary but insufficient condition for the better model resolution.

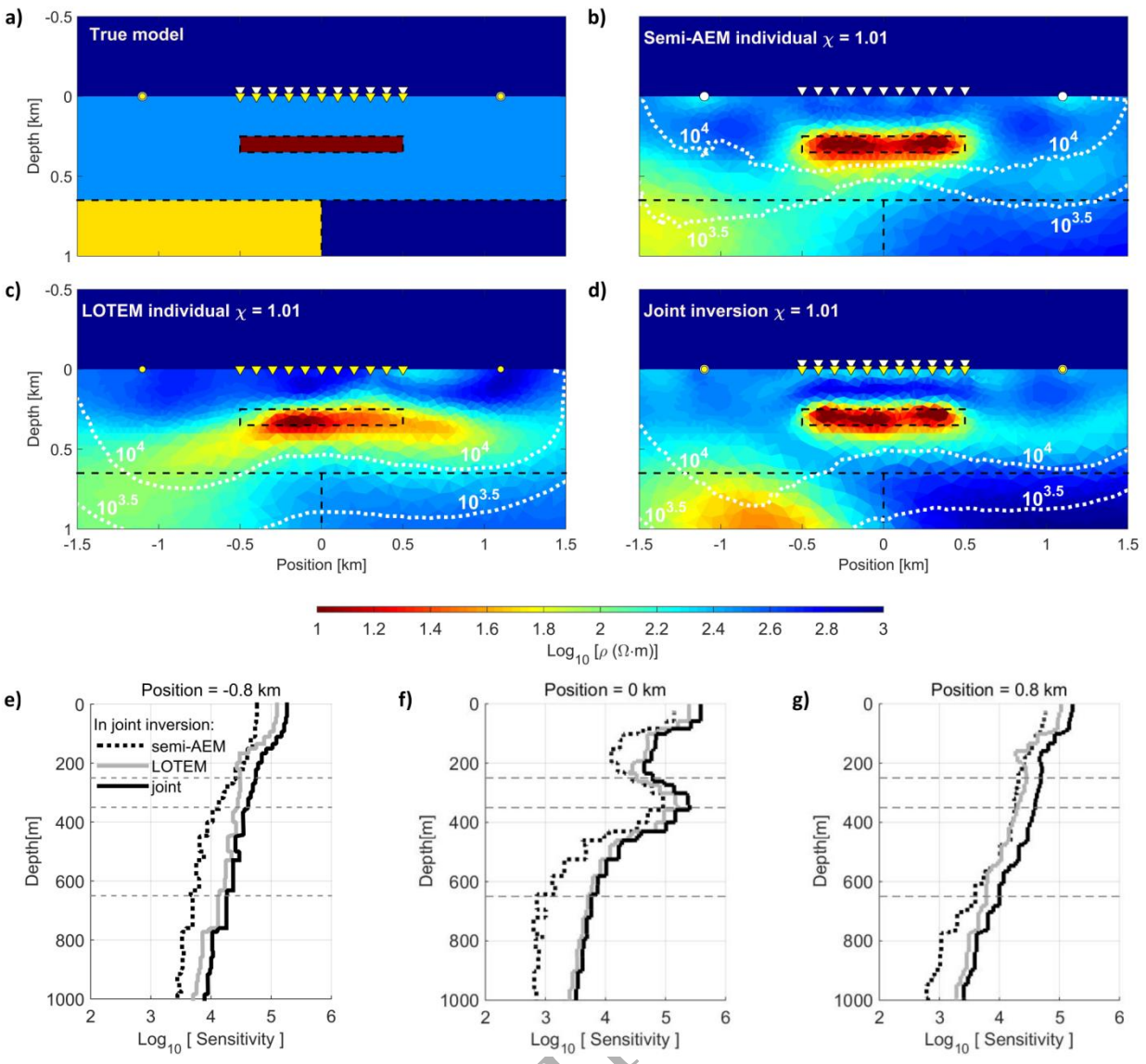

Figure 3. 2-D inversion results for the synthetic data of model shown in (a). Results are displayed for the inversions of (b) semi-AEM Tz individually, (c) LOTEM Ex step-on transient individually and (d) LOTEM and semi-AEM data jointly; the transmitters used for semi-AEM measurements are denoted as big white circles, those for LOTEM as small yellow circles; the white triangles in the air denote the semi-AEM receiver locations, and the yellow ones on land are LOTEM stations; the sensitivity contours at $10^{3.5}$ and 10^{4} are presented as white dotted-lines; (e), (f) and (g) compare the sensitivities as a function of depth for semi-AEM, LOTEM and both datasets in joint inversion (d) at the positions -0.8 km, 0 km, and 0.8 km, respectively. The black dashed-lines are the sensitivity of semi-AEM data for the resistivity model in (d); the grey solid lines are the sensitivity contributed by LOTEM data, and black solid lines are the sensitivity calculated for both datasets.

As indicated by the sensitivity contours, the cumulative sensitivities in the LOTEM individual inversion (Figure 3c) are stronger than those in the semi-AEM individual inversion (Figure 3b) for deep regions (> 650 m), but fairly similar to those in the joint inversion result (Figure 3d). However, this similarity does not guarantee that the LOTEM dataset also contributes to the sensitivity for the deep region in the joint inversion model (Figure 3d) because the resistivity model is different compared to the single inversion. Since the sensitivity contours in Figure 3d are calculated based on both the LOTEM and semi-AEM datasets, we clarify the cause of the better resolution of joint inversion result via a clear quantitative comparison. Figure 3e to 3g show sensitivity-depth models at three positions in the joint inversion result (Figure 3d) contributed by semi-AEM, LOTEM datasets and the combination of them, respectively. The overall characteristics are similar and consistent. However, it is clear that the sensitivity amplitude is enhanced in the deep region of joint inversion result due to LOTEM data contributions.

Given that the same transmitters and horizontal receiver positions used for both methods in this synthetic study, the stronger sensitivities of the LOTEM data are a product of inherent resolution characteristics of the electric field components and the lower error estimations. By including semi-AEM data to constrain the shallow structure of the joint inversion model, we limit the non-uniqueness of the inversion, which also provides a higher resolution of the basement resistivity structure obtained through the LOTEM data. The sensitivity of the LOTEM solo inversion model within the deep region is comparable to the joint inversion, yet the single inversion cannot replicate the true resistivity structure due to model ambiguity. Without constraining the shallow regions of the model by including semi-AEM data, the LOTEM data are fitted by an equivalent model that can include inversion artefacts in the shallow regions together with a poorly resolved basement structure.

In conclusion, the synthetic study shows that: (1) the code adaptation of MARE2DEM can be used to simultaneously interpret frequency- and time-domain CSEM data; (2) the semi-AEM vertical magnetic fields and the LOTEM electric fields show distinct resolution characteristics, although both transmitters and horizontal receiver offsets are identical; (3) although the sensitivity amplitudes of the semi-AEM data are

smaller than those of the LOTEM data, semi-AEM provide constraints on the shallow resistivity structure, enabling the joint inversion to replicate the true resistivity structure with a higher consistency compared to the individual inversion models.

4.2 2-D joint inversion of field data

Here we present the 2-D inversion results obtained from the semi-AEM and LOTEM data measured during the flight experiments in eastern Germany (Figure 1). The LOTEM and semi-AEM measurements are described in detail in Mörbe et al. (2020) and Smirnova et al. (2019), respectively. Since the semi-AEM survey covered only part of the LOTEM profile, the 2-D inversion study considers only the LOTEM stations located in the semi-AEM measurement area (blue dashed line in Figure 1) and semi-AEM data collocated along the LOTEM profile. As illustrated in Figure 1, LOTEM data correspond to 4 Txs, and two of them were used for semi-AEM measurement. The stations for both the LOTEM and the semi-AEM surveys were at intervals of about 100 m. The utilized largest offset was around 3300 m and 1400 m for LOTEM and semi-AEM, respectively. The LOTEM measurements were selected at 24 time points ranging from 0.0005 to 0.4 s, and the semi-AEM data were selected at 17 frequencies ranging from 58 Hz to 922 Hz. Due to the strong 3-D, IP, and possible anisotropic effects (cf. Liu et al., 2020) in the survey area, the error floor of LOTEM field data had to be increased to 5% (Mörbe, 2020). Since the errors of semi-AEM field data are usually larger than 5% for relatively low frequencies (e.g., 5% to 10% between 200 Hz to 50 Hz), they are still generally larger than the error estimations of LOTEM field data. The 1000 Ωm half space is used as the starting model for the field data inversion. Figure 4a to 4c present the inversion results. All the results were obtained after 25 inversion iterations.

Prior to the inversion of the semi-AEM field data, we tested several horizontal-vertical smoothing weights from 1 to 100. The final resistivity models were generally consistent. In the semi-AEM inversion model (Figure 4a), four conductive structures are presented. They are highlighted by black dashed lines and marked as C1 – C4. The shallow conductive bodies C1, C2 and C3 were also revealed by helicopter EM (HEM) measurements (Steuer et al., 2020). However, the depth extension of C2 could not be validated by HEM due

to its limited depth of investigation. The anomaly C4 is located at a depth of approximately 500 m, beneath C2.

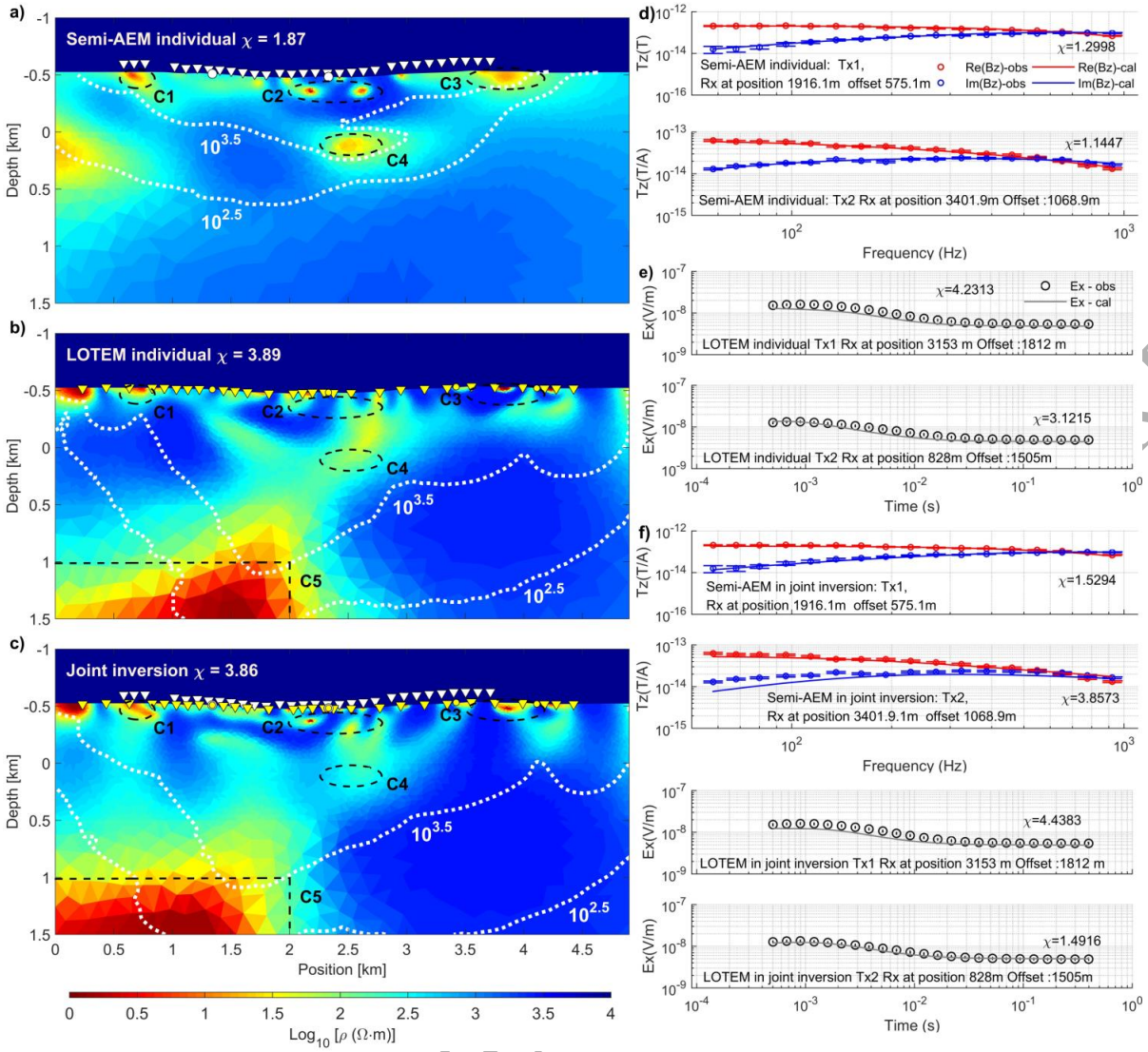

Figure 4. 2-D inversion results for the field data acquired in eastern Thuringia, Germany. Results are displayed for the inversions of (a) semi-AEM T_z individually, (b) LOTEM Ex step-on transient individually and (c) LOTEM and semi-AEM data jointly. The dotted white contours of the sensitivity overlay the resistivity models. The main conductors are highlighted by black dashed lines and marked as C1 – C5. Panels (d), (e) and (f) present the examples of the data misfit at selected stations for semi-AEM and LOTEM individual inversions and for joint inversion.

The inversion model obtained from the LOTEM data (Ex) is shown in Figure 4b. The data misfit for the LOTEM inversion is larger (3.89) than that of the semi-AEM inversion (1.87). Reasons for the larger data misfit of LOTEM include e.g., 3D, anisotropy or IP effects, as well as the larger error bars of semi-AEM. The resistivity anomalies detected by the semi-AEM inversion as illustrated in Figure 4a are indicated by black dashed lines. Qualitatively, the resistivity structure from the single LOTEM inversion shows similarities to the inversion model of semi-AEM data. The conductive structures labelled C1 to C3 are also recovered by the LOTEM inversion. However, significant discrepancies between semi-AEM and LOTEM results are found within the deeper regions of the model. Conductor C4 extends into a continuous conductive zone in Figure 4b. A further conductive structure (C5), which is not observable in the semi-AEM inversion at a depth greater than 1 km appears in the LOTEM model between the horizontal position of 0 to 2.5 km.

The joint inversion of the semi-AEM and LOTEM field data converged to a total misfit of 3.86 for both datasets (Figure 4c), while the separated misfits for each dataset are 2.89 for semi-AEM and 4.24 for LOTEM. The joint inversion modelling took approximately 12 days of computing time using 96 processors on the HPC of the University of Cologne. The majority of the computational resources were consumed by the LOTEM calculations. Figure 4d to 4f show a comparison of the data misfit at selected stations between single method inversions and joint inversion. The resistivity distributions shown in Figure 4c are dictated by the LOTEM data and appear similar to those in Figure 4b. The similarities include the deep structure C5 and the absence of the isolated C4 anomaly. The amplitudes of the total sensitivity distributions are also mainly dominated by LOTEM data in the joint inversion.

An interpretation of the subsurface structures in the survey area is provided by Steuer et al. (2020), where geological and petro-physical information were utilized to interpret the obtained geophysical inversion models. According to Steuer et al. (2020), high conductive structures below 10 Ωm can be related to the presence of alum shales, whereas resistive regions can be interpreted as Ordovician clay and silt shales in the shallow subsurface followed by Ordovician phyllites and quartzite at greater depth.

4.2.1 Model validation using forward data

To investigate the robustness of the structures derived from the 2-D joint inversion, further synthetic tests are conducted. Here, we inverted the calculated data from Figure 4c separately for semi-AEM and LOTEM data to investigate if the discrepancies in the inversion models are due to resolution differences. The inversion parameters and the inversion mesh were kept the same as those used in the field data inversion. The resulting inversion models of this study are shown in

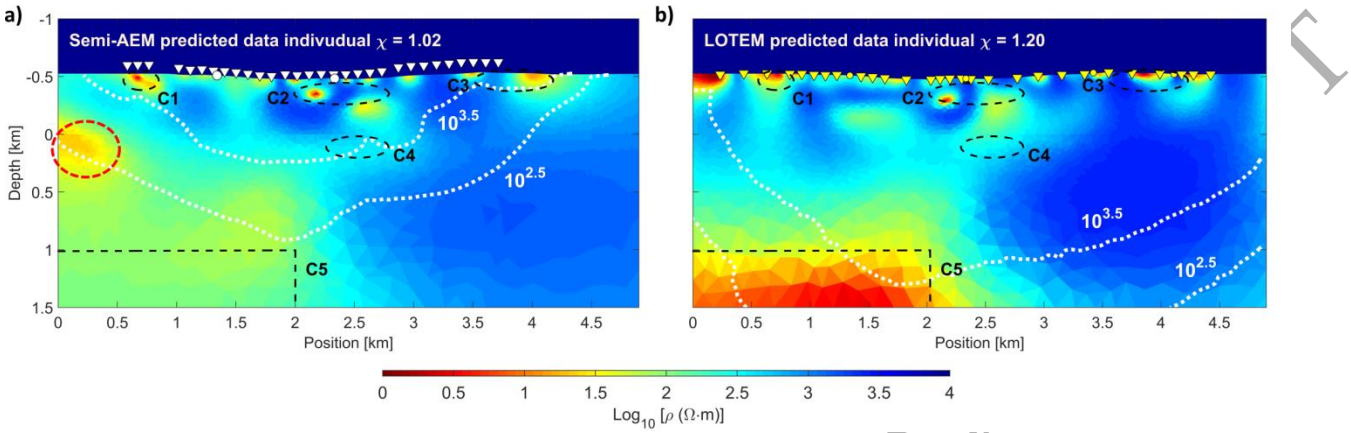

Figure 5a and 5b for semi-AEM and LOTEM data, respectively. For the LOTEM inversion

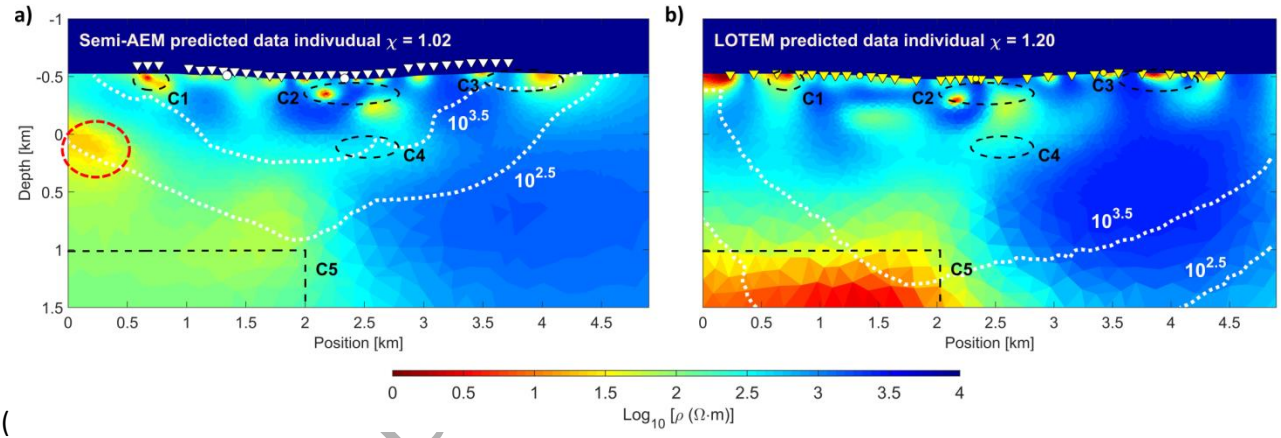

(

Figure 5b), the general resistivity distribution is comparable to that of the joint inversion result of the field data aside from slight distinctions in shallow layers. This similarity shows that reconstructing the resistivity model in Figure 4c is feasible and consistent using the applied LOTEM configuration.

For the semi-AEM inversion, the resistivity distributions in Figure 4a and

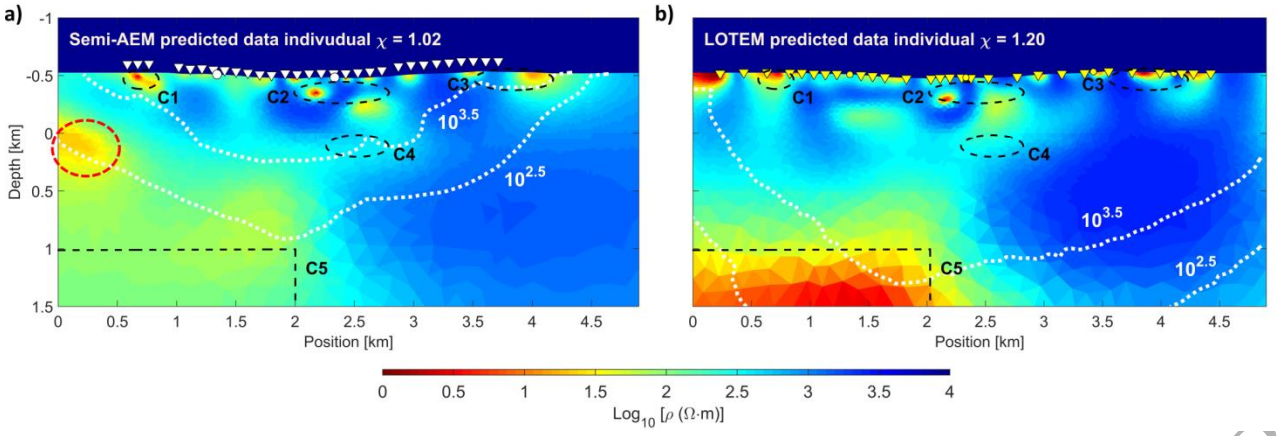

Figure 5a show a strong similarity within the shallow subsurface. For instance, the C2 anomaly has a similar shape to that in Figure 4a. Moreover, the conductor located between the depths of 0 to 0.5 km is also present (highlighted by the red dashed line in

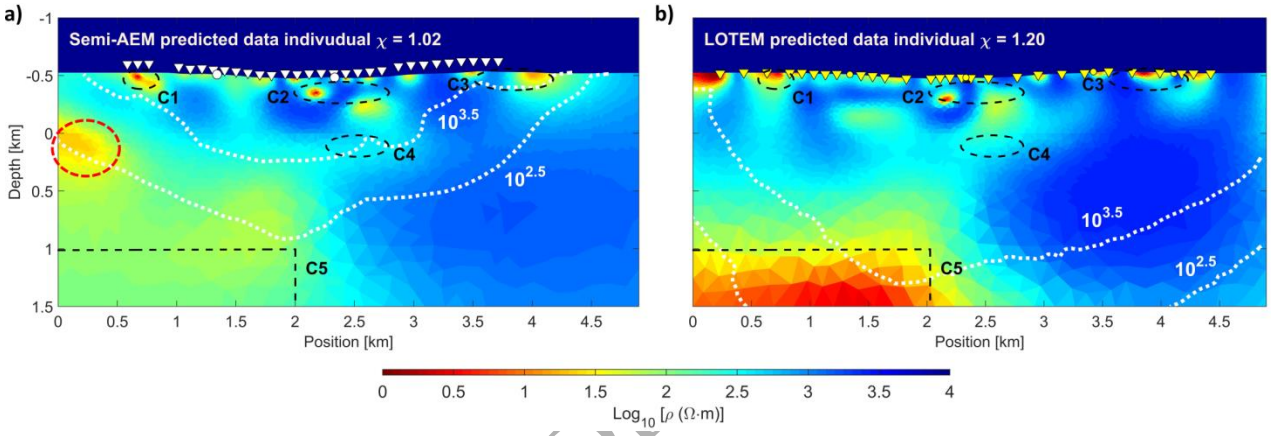

Figure 5a). These results suggest that, for the shallow subsurface, the joint inversion is influenced by the information from the semi-AEM data. The discrepancy in the shallow regions between the semi-AEM inversion and the joint inversion can be explained by the resolution differences of semi-AEM and LOTEM datasets. For example, C3 is not covered by semi-AEM stations, which results in a decreased resolution. Hence, C3 is only qualitatively imaged by the semi-AEM inversion. Another example is the conductor highlighted by the red dashed line in

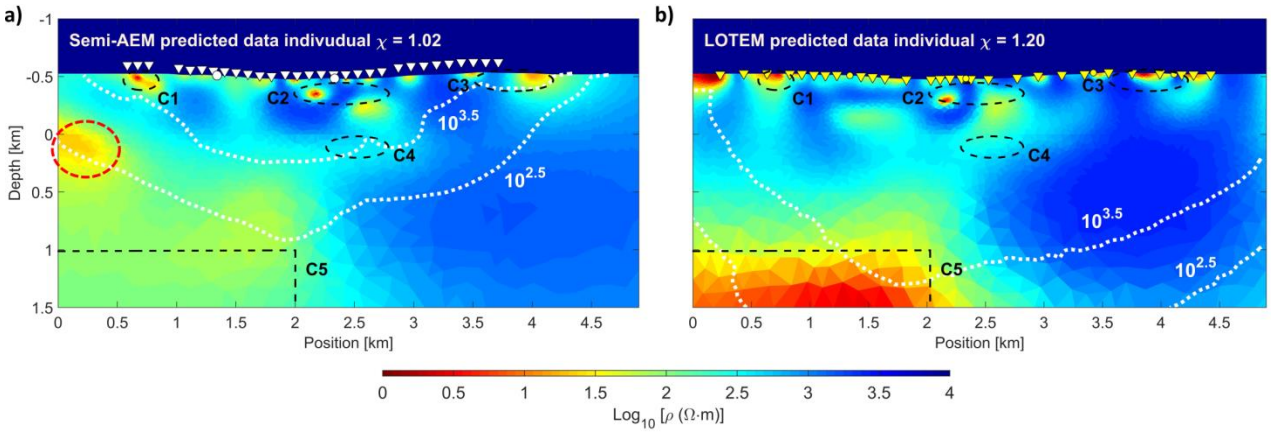

Figure 5a. It appears in the field data inversion result (Figure 4a) but disappeared in the joint inversion (Figure 4c). When the semi-AEM predicted data were inverted individually

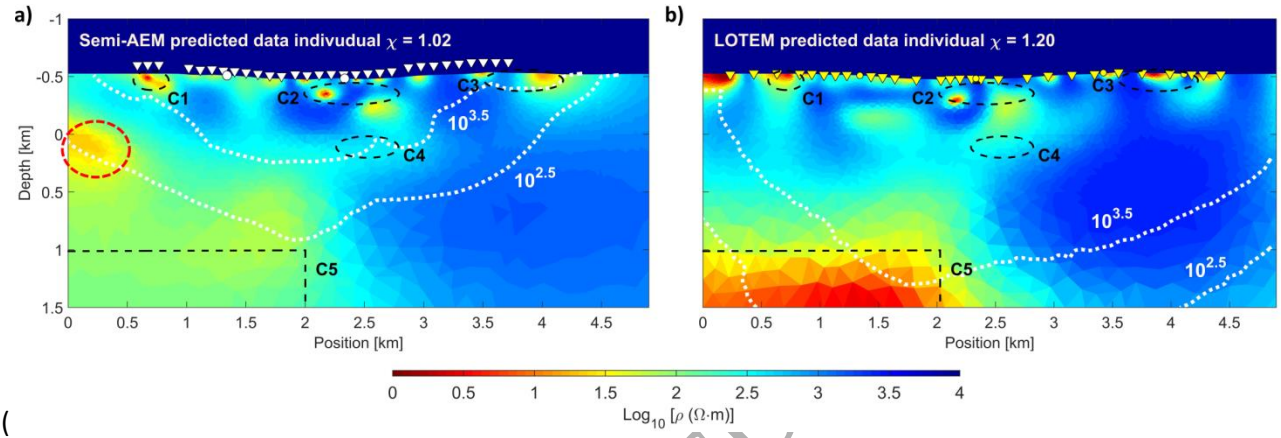

(

Figure 5a), this conductor appears again.

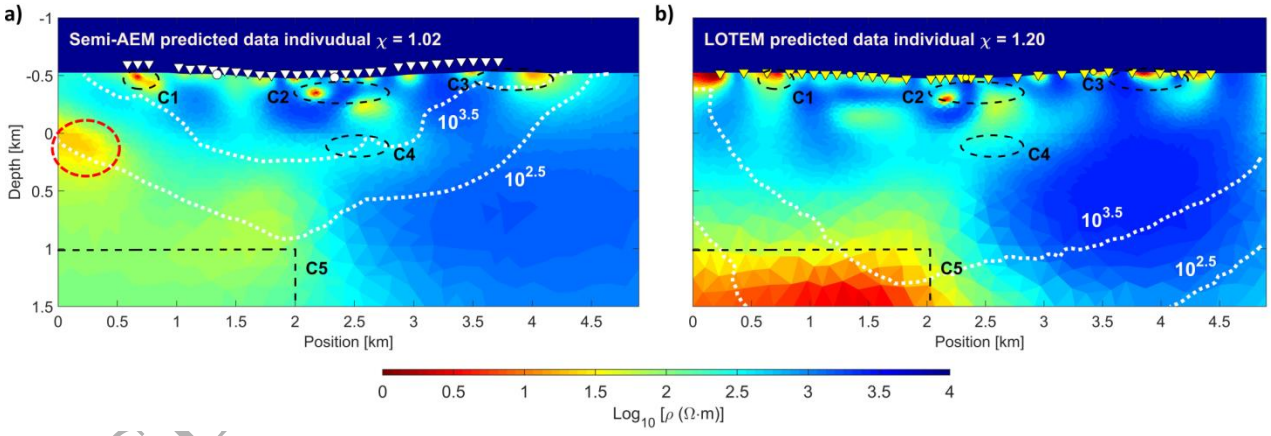

Figure 5. Inversion models of the predicted data of the resistivity model obtained in field data inversion (Figure 4 c). (a) semi-AEM Tz individually, (b) LOTEM Ex step-on transient individually. The white dotted

contours depict the cumulative sensitivity of the inversion model for each method. The conductors C1 – C5 illustrated in Figure 4c are denoted by black dashed lines for comparison.

Figure 4a and

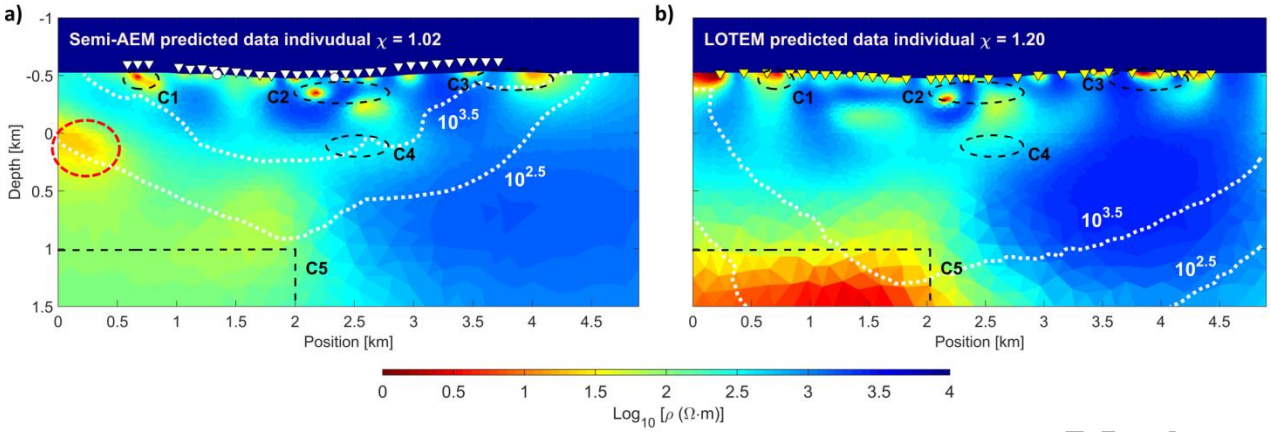

Figure 5a also show some disagreement for deeper structures. For example, a conductive zone is observable around C5 in

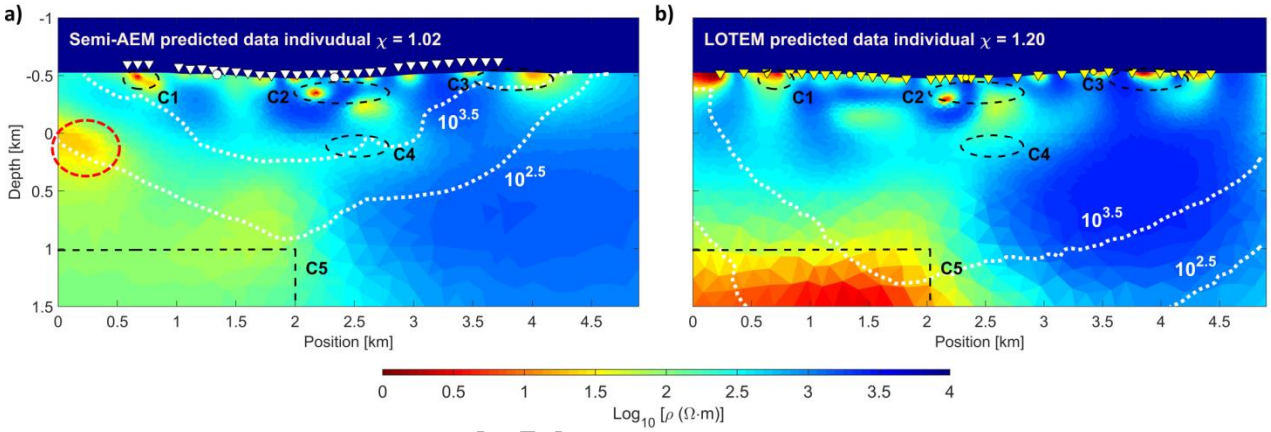

Figure 5a. The semi-AEM data have poor resolution for the structures at this depth, but still can be slightly affected by them. This disagreement may suggest that different information about the deep structure is contained in the semi-AEM field data and in the predicted semi-AEM data of the joint inversion model. The appearance of conductive zone around C5 is caused by the information from LOTEM data which is introduced into predicted data via the joint inversion. However, the C5 anomaly is suggested by LOTEM data solely, and it locates at the edge of the model and might therefore be a side effect from adjacent anomalies located outside the profile or an artefact caused by other unconsidered factors. A further disagreement

between the models of Figure 4a and

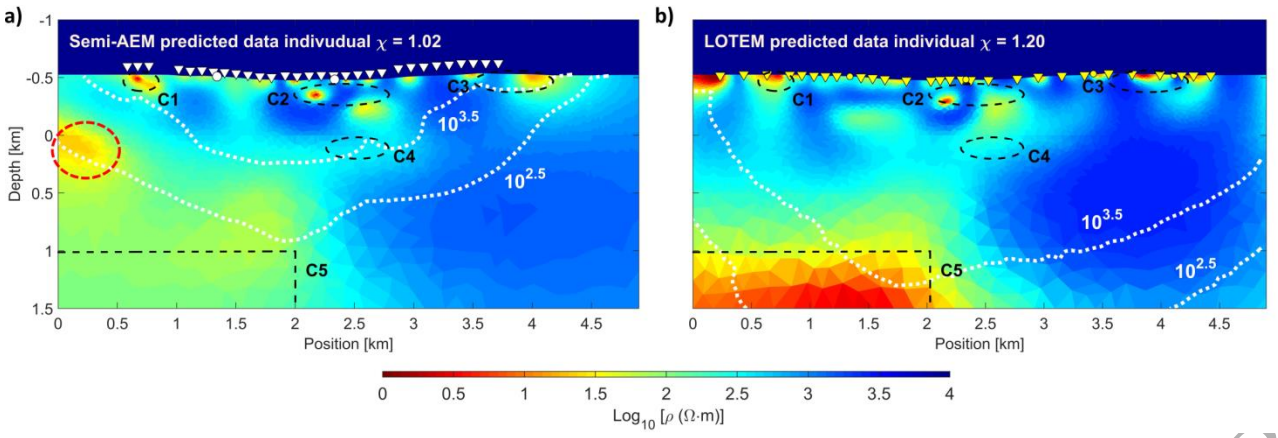

Figure 5a is the absence of C4 observable in the inversion of semi-AEM field data (Figure 4a). Different from the conductor marked by the red dashed circle in

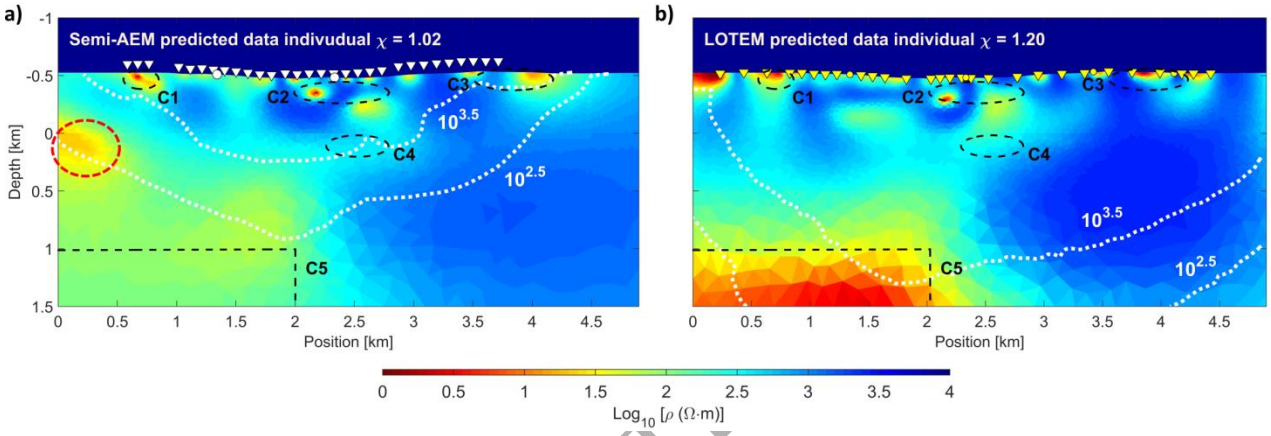

Figure 5a, C4 is not shown again by the individual inversion, indicating the reason for its absence in joint inversion (Figure 4c) is not only the resolution differences. C4 and C5 are not imaged by both datasets and therefore cannot be confirmed; these features may be a product of exclusive information within the individual datasets and may come from factors not considered in this study, such as the effects caused by anisotropy, induced polarization or 3D effects.

The information obtained in this synthetic modelling study shows that the shallow region of the 2-D joint inversion result from the field data is influenced by both semi-AEM and LOTEM data. In turn, the LOTEM data provide information about the deeper region (> 500 m). However, note that the information about

deeper regions (i.e from. long period data) might be affected more by 3D effects and no other independent information can be provided for additional validation.

4.2.2 Model validation using a simplified synthetic field data model

Since complex minor structures in the inversion results of the field data make a more insightful analysis challenging, we analyse a simplified version of Figure 4c in the following (Figure 6a). The synthetic model in Figure 6a consists of a 1000 Ωm background layer and four conductive targets with a resistivity of 10 Ωm. The three small conductive bodies buried close to the earth's surface correspond to C1 - C3. C5 is simulated by a rectangular conductive body buried at a depth of about 1500 m. The measurement configurations of the field data are employed, and the true topography is considered. Also, the synthetic data were computed for the same frequencies and time points as those of the measured data. To validate the result in Figure 4c, we investigate if satisfactory inversion results are achievable for the synthetic model (Figure 6a) by using the field configurations employed above. Figure 6b to 6d show the results of the 2-D inversions applied to the synthetic data. Note that the 2-D inversions were terminated if the χ = 1.0 or the maximum number of iterations (40) was reached.

The single semi-AEM inversion (Figure 6b) converged to the desired χ = 1.0 after 20 iterations. As presented in Figure 6b, the employed semi-AEM field configuration can detect the three shallow conductors C1 to C3. The deep conductive structure C5 is absent, which can be explained by the relatively small sensitivity of semi-AEM data at this depth. However, an artificial conductive body appears above the original position of C5, which could imply a slight perturbation on the semi-AEM data caused by C5. This perturbation could also lead to the expanded C1 in Figure 6b. In an additional synthetic modelling where the structure C5 is removed from the true model, the artefacts around C5 and C1 disappear in the semi-AEM single inversion.

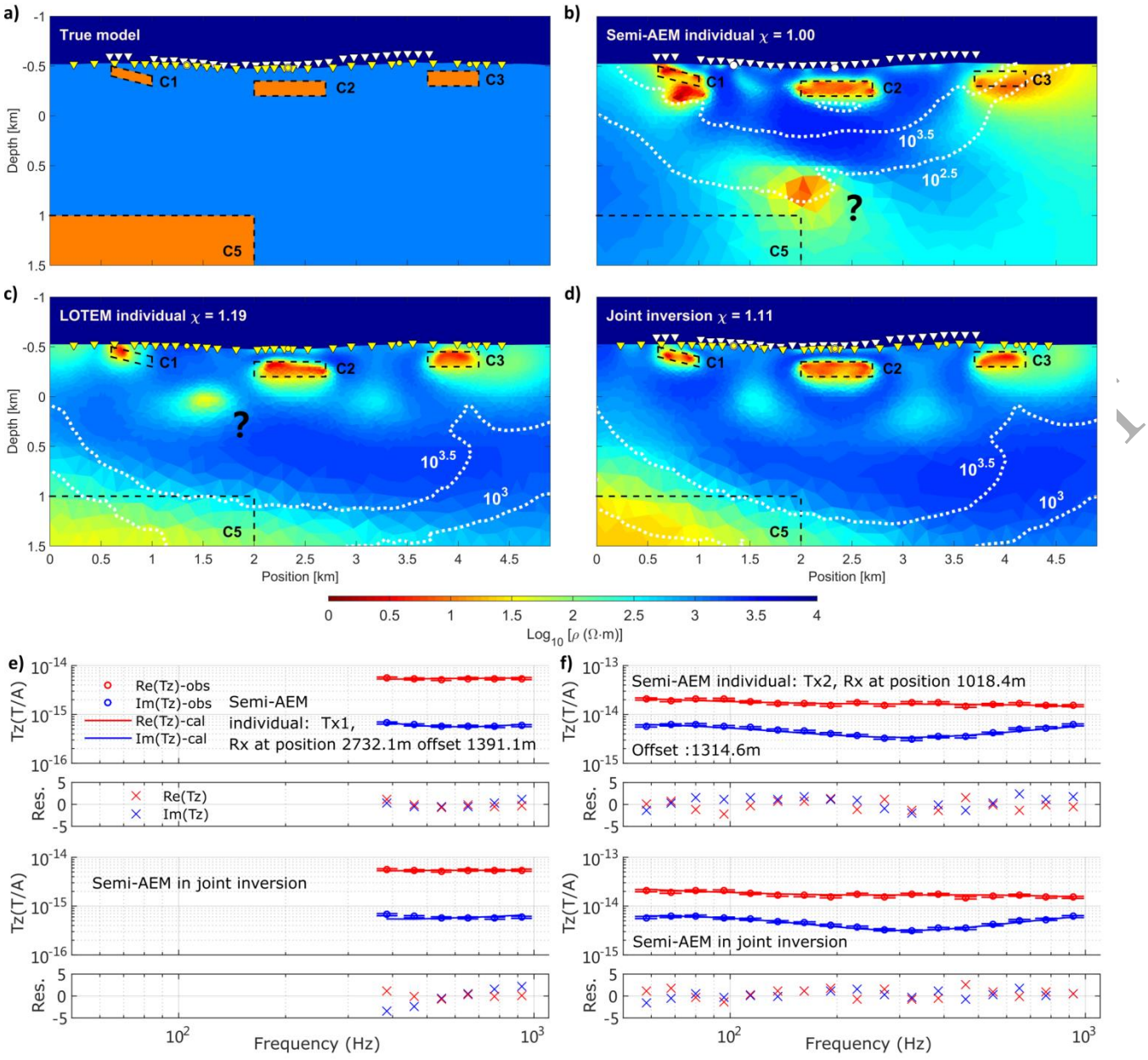

Figure 6. 2-D inversion results for the synthetic data of model shown in (a). The resistivity model in (a) is a simplification of the joint inversion result in Figure 4c. 2-D inversion results are displayed for the inversions of (b) semi-AEM T_z individually, (c) LOTEM Ex step-on transient individually and (d) LOTEM and semi-AEM data jointly; the white dots contour the sensitivity in the subfigures; (e) and (f) present the data misfit for two selected stations with large offsets.

The 2-D inversion of only LOTEM electric fields (Figure 6c) reached χ = 1.19 after 40 iterations. Due to the stronger sensitivities at depths greater than 1 km, the background resistivity is resolved more clearly.

However, manifold artificial structures also occur. An artefact with a resistivity of about 30 Ωm appears between the horizontal positions of C1 and C2 (at a depth of 0 km). Moreover, C1 is not fully revealed on the right side but extended on the left side.

The 2-D joint inversion reached a total $\chi = 1.11$ after 40 iterations. The joint inversion result shown in Figure 6d resolved all the target conductors. The artefact above C5 in Figure 6b disappears by including the LOTEM data. In turn, the artefact in Figure 6c is less apparent due to the semi-AEM data. Figure 6e and 6f compare the data fit between the semi-AEM inversion and the joint inversion at the largest offsets above the C5 structure.

This study demonstrates the nature of the ill-posed EM problem. Due to non-uniqueness, artefacts are produced in the inversion that can be easily misinterpreted. Especially for large scale and deep EM applications, the derived models need to be tested for the robustness and reliability of the reconstructed structures. Although the inversion results shown in Figure 6b and c may vary if different inversion parameters are used, considering more independent information via a joint inversion can reduce the equivalence domain and lead to more stable and reliable inversion results. This synthetic result also demonstrates the feasibility of revealing the four discussed conductive targets through the 2-D joint inversion. Therefore, the joint inversion result of the field data in Figure 4c could be considered at least as one possible interpretation of the discussed two field datasets. Unfortunately, the conductor C5 is not clearly depicted in Figure 6d, neither for the rectangle-like boundary nor for the true resistivity values, even though the sensitivities around C5 in this synthetic example are stronger than those in Figure 4c or

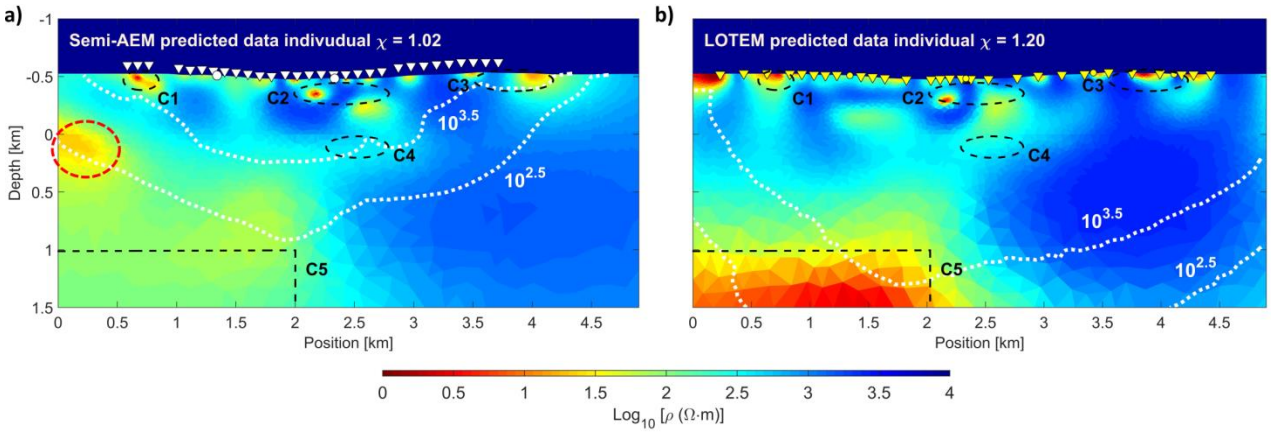

Figure 5b.

4.3 2-D joint inversion with a reduced LOTEM configuration

As described earlier, the semi-AEM approach allows a large measurement area to be covered efficiently. On the other hand, ground-based LOTEM measurements (or generally CSEM) commonly provide better data quality; thus, larger offsets and a higher penetration depth can be achieved to validate and constrain the densely-measured semi-AEM data. LOTEM data can improve the general resolution of inversion results, especially for deep structures. However, the drawbacks of any joint measurement are also obvious — more extensive field work is necessary and a larger computational load during data evaluation. To reduce the costs of multi-dimensional joint inversions, the feasibility of reducing the required LOTEM stations is investigated. Since LOTEM measurements are usually time-consuming and restricted in harsh terrain, decreasing the number of LOTEM stations will reduce the acquisition time and make the field survey more efficient. Therefore, we investigated for the given dataset if the advantages of joint inversion can be maintained while the number of ground-based stations is reduced. To answer this question, LOTEM stations with an offset of less than 2500 m were removed from the 2-D joint inversion, since for those offsets additional semi-AEM data are present. The schematic views of the full LOTEM configuration and the reduced configuration are illustrated in Figure 7a and b, respectively. By using the reduced configuration, 80% of the LOTEM stations are omitted, and the number of LOTEM data points is reduced from 1680 to 336. The 2-D joint inversion result of the semi-AEM data and the reduced LOTEM dataset is displayed in Figure 7c. Although only 20% of the LOTEM data are considered, the joint inversion result shows no significant difference than Figure 6d. All

four target conductors are clearly resolved, even though the sensitivities are generally smaller. Due to the reduced computation load, the inversion converged to $\chi = 1.01$ in 25 iterations.

As indicated, for this simple synthetic model, the joint inversion of data from the semi-AEM and reduced LOTEM set-up is enough to provide a resistivity model reconstructing all main structures without showing additional artefacts. To further investigate the minimum required ground stations, we considered the extreme case when only one LOTEM station is included. The LOTEM station with the largest offset (marked by a red arrow in Figure 7b) was employed to provide information about the deep structures . As shown in Figure 7d, the artefacts resulting only from the semi-AEM inversion (Figure 6b) are constrained even though only one LOTEM station is considered. Nevertheless, the information from one LOTEM station is not enough to clearly resolve the C5. If an additional LOTEM station at a large offset but with a different Tx-Rx configuration is considered (marked by a blue arrow in Figure 7b), the obvious improvement can be seen in the reconstruction of C5. In Figure 7e, the deep conductive area below 100 Ωm is constrained to the left side of position 2 km (Figure 7d). Subsequently, the resolution of the C5 structure will increase if more LOTEM stations with large offsets are considered in the inversion, for example, the case shown in Figure 7c. Note that C3 is not covered by semi-AEM CSEM data and is poorly reconstructed when using only one or two LOTEM stations.

Sensitivity calculations for reduced LOTEM configurations

To evaluate the sensitivity variations when different LOTEM configurations are considered in the joint inversions, we compared sensitivities as a function of depth at four different positions (Figure 7f to i). The sensitivities of 2-D joint inversions with different LOTEM configurations are identical to those presented by white contours in Figure 6d, Figure 7c, d and e, correspondingly. As expected, sensitivities are enhanced if more stations are included. In detail, the sensitivity variations illustrate the differences in the inversion results (Figure 7c to 7e and Figure 6d). Between the cases of one-Rx and two-Rxs (grey and black dots), the sensitivity enhancements focus beneath 800 m at the position 1 km to 3 km. These stronger sensitivities in the deep region support better resolution of C5 in the two-Rxs case. The generally enhanced sensitivities at 4

km (Figure 7i) between one-Rx and two-Rxs cases also explain the resolved right-side background in the model (Figure 7e).

After including the LOTEM stations with offsets larger than 2500 m (denoted as a reduced configuration, grey solid line) in the joint inversion, the sensitivities are generally strengthened for the deep region. In the comparison with the case of a reduced LOTEM configuration, the sensitivity enhancements led by the full LOTEM configuration (black solid line) are always larger in the shallow area than in the deep area. Particularly, the sensitivity increase derived from the full LOTEM configuration is slightly below the depth of 1000 m at 1 km (Figure 7f, in the middle of C5), supporting the view that the data from short offsets are not necessary when densely acquired semi-AEM data are available.

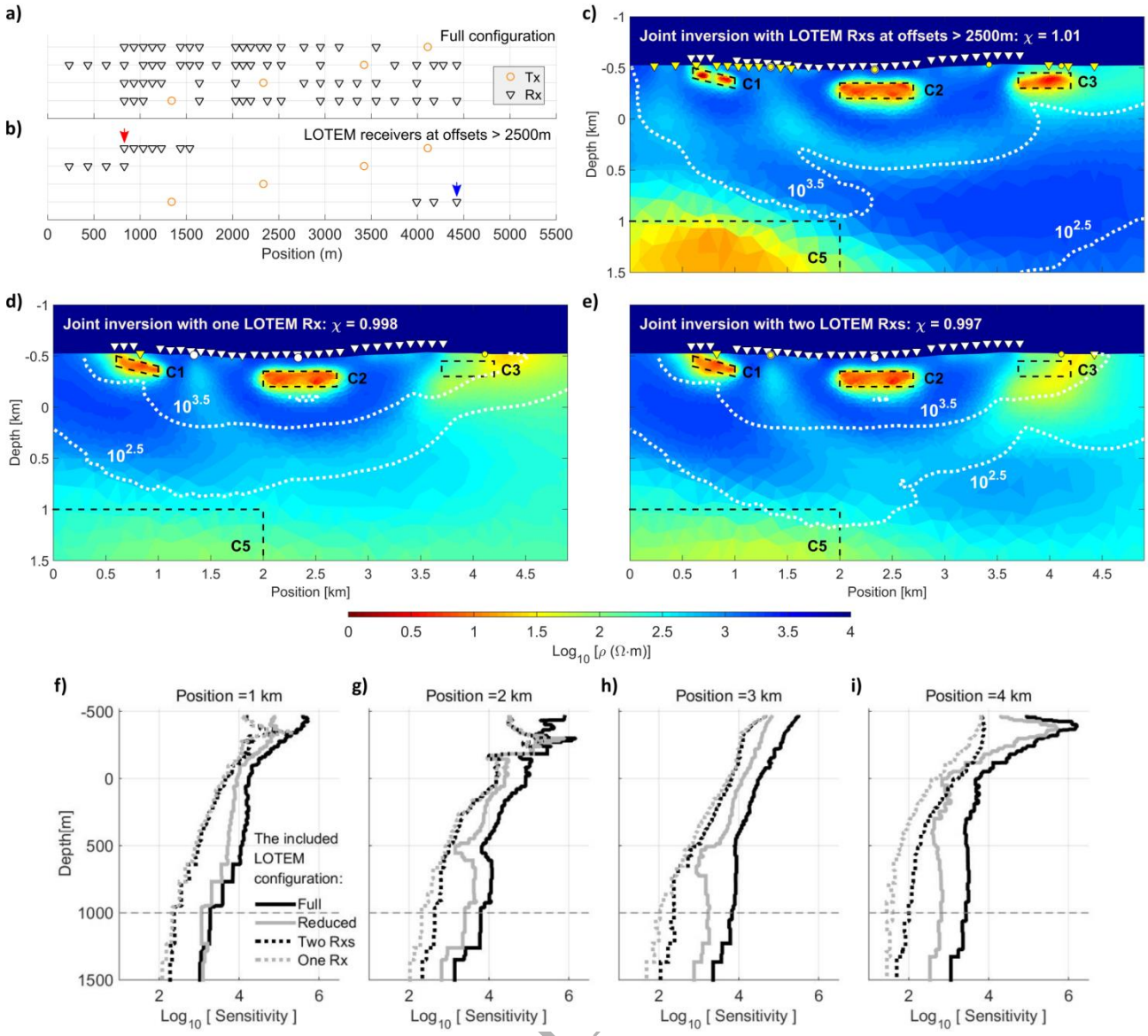

Figure 7. 2-D joint inversion results for the semi-AEM and the reduced LOTEM datasets. The true model is in Figure 6a. (a) displays the full LOTEM configuration considered in Figure 6d, and (b) displays the reduced LOTEM configuration; in each line, the utilized transmitter (orange circles) and the corresponding receiver positions (black triangles) are displayed. (c) displays the 2-D joint inversion results using the reduced LOTEM dataset; (d) displays the 2-D joint inversion results using the data from only one LOTEM station, which is marked by a red arrow in (b); (e) displays the 2-D joint inversion results using the data from two LOTEM stations (the two stations are marked by red and blue arrows); the white dots contour the sensitivity in the subfigures; (f), (g), (h) and (i) compare the sensitivities of joint inversions including different LOTEM configurations for vertical positions 1, 2, 3 and 4 km, respectively.

For this specific example, only one deep target needs the supplementary information from the electric step-on Ex signal at large offsets. Therefore, the reduced LOTEM configuration in Figure 7b with offsets larger than 2.5 km could be one optimal choice. Broadly, the additional LOTEM stations in a semi-AEM survey bring independent information and possibly improve resolution, but also add more costs in time and field work. Sometimes, a small amount of key supplemental information from ground stations may play an essential role in resolving deep structures and avoiding artefacts. In addition, sparse land-based stations at short offsets can be deployed to constrain the shallow layers, for example in a more complex case. This synthetic modelling study suggests using a careful selection and planning of land-based configurations in a joint semi-AEM and LOTEM survey. Especially, in difficult terrain and logistics, the survey efforts can be optimally minimized.

5 Conclusion

Here, we presented the 2-D joint inversions of LOTEM electric fields in the time domain and magnetic fields of the newly developed semi-AEM system in the frequency domain. The semi-AEM system combines ground-based transmitters with AEM magnetic field receivers. Therefore, it can cover the measuring area efficiently while reaching a depth of investigation of about 1 km. The conventional LOTEM measurement provides complementary information from electric fields, especially those measured at large offsets. A joint inversion of both datasets can therefore help to constrain subsurface structures and can provide enhanced resolution in the inversion results.

The open-source 2-D modelling code MARE2DEM was adapted to fulfil the 2-D joint inversion requirements of frequency- and time-domain data for HED sources and was then applied to the field data acquired in eastern Thuringia, Germany. Although the 2-D inversion results show obvious divergences for the individual methods, the 2-D joint inversion of the LOTEM and semi-AEM field data converge successfully. As indicated by further synthetic studies, part of the discrepancies among the 2-D inversion results can be explained by the resolution difference of the two datasets. Not only the different observed quantities and error

estimations but also the diverse measurement configurations play an important role in the resolution characteristics. The general validity of the joint inversion result of the field data was confirmed by the synthetic studies from the perspective of feasibility. However, part of the discrepancies in the inversion results cannot be explained by the resolution differences only, and some revealed structures are still unclear. These undetermined problems could be the influence of the unconsidered factors, such as 3-D structures, anisotropic or IP effects. In the frame of a 2-D joint inversion of semi-AEM and LOTEM, flexible land-based configurations with fewer land-based stations than usual could be employed to reduce survey costs or overcome some harsh environmental conditions.

Acknowledgement

We thank the editor and the three reviewers, Dr. Mathias Scheunert, Dr. Mehmet Emin Candansayar, and Dr. Dikun Yang, for their suggestions which helped us to significantly improve the manuscript. We would like to thank the field team of the DESMEX Survey 2016 and 2017 and the DESMEX work group. DESMEX is funded by the Federal Ministry of Education and Research (BMBF) under BMBF grant 033R130. The SPAM Mk IV System used for the acquisition of the LOTEM data was provided by the Geophysical Instrument Pool Potsdam (GIPP, grant numbers 201608). Cai Ji was funded by the Chinese Scholarship council program (no. 201506330059). All 2-D inversion models were computed at the HPC Facilities provided by the University of Cologne.

Data availability

Underlying this article, the LOTEM field data acquired in 2016 in eastern Thuringia, Germany are in parts available in GFZ Data Services, at https://doi.org/10.5880/GIPP-MT.201608.1. Additional LOTEM data will be shared on reasonable request to Wiebke Mörbe. The semi-AMT field data will be shared on reasonable request to Maria Smirnova and Michael Becken. The other synthetic modelling data will be shared on reasonable request to the corresponding author.

Reference

Anderson, W. L., 1982, Fast Hankel Transforms Using Related and Lagged Convolutions: ACM Transactions on Mathematical Software, v. 8, no. 4 p. 344–368.

Becken, M., Nittinger, C. G., Smirnova, M., Steuer, A., Martin, T., Petersen, H., Meyer, U., Mörbe, W., Yogeshwar, P., Tezkan, B., Matzander, U., Friedrichs, B., Rochlitz, R., Günther, T., Schiffler, M., and Stolz, R., 2020, DESMEX: A novel system development for semi-airborne electromagnetic exploration: Geophysics, v. 85, no. 6, p. E253-E267.

Cai, J., 2020, Development of 1D and 2D Joint Inversion Algorithms for Semi-Airborne and LOTEM Data: A Data Application from Eastern Thuringia, Germany. [Ph.D. thesis]: University of Cologne.

Cai, J., Tezkan, B., and Li, Y., 2018, Effects of the sea floor topography on the 1D inversion of time-domain marine controlled source electromagnetic data: Geophysical Prospecting, v. 66, no. 8, p. 1602-1624.

Commer, M., Helwig, S. L., Hördt, A., and Tezkan, B., 2005, Interpretation of long-offset transient electromagnetic data from Mount Merapi, Indonesia, using a three-dimensional optimization approach: Journal of Geophysical Research, v. 110, no. B03207.

Commer, M., and Newman, G. A., 2009, Three-dimensional controlled-source electromagnetic and magnetotelluric joint inversion: Geophysical Journal International, v. 178, no. 3, p. 1305-1316.

Constable, S. C., Parker, R. L., and Constable, C. G., 1987, Occam's inversion: A practical algorithm for generating smooth models from electromagnetic sounding data: Geophysics, v. 52, no. 3, p. 289-300.

Gehrmann, R. A. S., Schwalenberg, K., Riedel, M., Spence, G. D., Spiess, V., and Dosso, S. E., 2016, Bayesian inversion of marine controlled source electromagnetic data offshore Vancouver Island, Canada: Geophysical Journal International, v. 204, no. 1, p. 21-38.

Haroon, A., Adrian, J., Bergers, R., Gurk, M., Tezkan, B., Mammadov, A. L., and Novruzov, A. G., 2015, Joint inversion of long-offset and central-loop transient electromagnetic data: Application to a mud volcano exploration in Perekishkul, Azerbaijan: Geophysical Prospecting, v. 63, no. 2, p. 478-494.

Haroon, A., Hölz, S., Weymer, B., Tezkan, B., and Jegen, M., Calculating Time-Domain Controlled Source Electromagnetic Signals with MARE2DEM, *in* Proceedings 3rd Applied Shallow Marine Geophysics Conference2018a, Volume 2018, European Association of Geoscientists & Engineers, p. 1-5.

Haroon, A., Lippert, K., Mogilatov, V., and Tezkan, B., 2018b, First application of the marine differential electric dipole for groundwater investigations: A case study from Bat Yam, Israel: Geophysics, v. 83, no. 2, p. B59-B76.

Kaufman, A. A., and Keller, G., 1983, Frequency and transient soundings, v. 7.

Key, K., 2016, MARE2DEM: a 2-D inversion code for controlled-source electromagnetic and magnetotelluric data: Geophysical Journal International, v. 207, no. 1, p. 571-588.

Key, K., and Ovall, J., 2011, A parallel goal-oriented adaptive finite element method for 2.5-D electromagnetic modelling: Geophysical Journal International, v. 186, no. 1, p. 137-154.

Li, Y., and Key, K., 2007, 2D marine controlled-source electromagnetic modeling: Part 1 — An adaptive finite-element algorithm: Geophysics, v. 72, no. 2, p. WA51-WA62.

Liu, Y., Yogeshwar, P., Hu, X., Peng, R., Tezkan, B., Mörbe, W., and Li, J., 2020, Effects of electrical anisotropy on long-offset transient electromagnetic data: Geophysical Journal International, v. 222, no. 2, p. 1074-1089.

Meju, M. A., 1996, Joint inversion of TEM and distorted MT soundings: Some effective practical considerations: Geophysics, v. 61, no. 1, p. 56-65.

Meqbel, N., and Ritter, O., 2015, Joint 3D inversion of multiple electromagnetic datasets: Geophysical Prospecting, v. 63, no. 6, p. 1450-1467.

Moghadas, D., Engels, M., and Schwalenberg, K., 2015, 1D joint multi-offset inversion of time-domain marine controlled source electromagnetic data: Geophysical Prospecting, v. 63, no. 6, p. 1334-1354.

Mogi, T., Kusunoki, K. i., Kaieda, H., Ito, H., Jomori, A., Jomori, N., and Yuuki, Y., 2009, Grounded electrical-source airborne transient electromagnetic (GREATEM) survey of Mount Bandai, north-eastern Japan: Exploration Geophysics, v. 40, no. 1, p. 1-7.

Mogi, T., Tanaka, Y., Kusunoki, K. i., Morikawa, T., and Jomori, N., 1998, Development of Grounded Electrical Source Airborne Transient EM (GREATEM): Exploration Geophysics, v. 29, no. 1-2, p. 61-64.

Moorkamp, M., Heincke, B., Jegen, M., Roberts, A. W., and Hobbs, R. W., 2011, A framework for 3-D joint inversion of MT, gravity and seismic refraction data: Geophysical Journal International, v. 184, no. 1, p. 477-493.

Mörbe, W., 2020, Deep Controlled Source Electromagnetics for Mineral Exploration: A Multidimensional Validation Study in Time and Frequency Domain. [Ph.D. thesis]: University of Cologne.

Mörbe, W., Yogeshwar, P., and Tezkan, B., 2021, Deep electromagnetic sounding for mineral exploration: LOTEM Validation Study 2016: GFZ Data Services.

Mörbe, W., Yogeshwar, P., Tezkan, B., and Hanstein, T., 2020, Deep exploration using long‐offset transient electromagnetics: interpretation of field data in time and frequency domain: Geophysical Prospecting, v. 68, no. 6, p. 1980-1998.

Peng, R., Yogeshwar, P., Liu, Y., and Hu, X., 2021, Transdimensional Markov Chain Monte Carlo joint inversion of direct current resistivity and transient electromagnetic data: Geophysical Journal International, v. 224, no. 2, p. 1429-1442.

Schwalenberg, K., Rath, V., and Haak, V., 2002, Sensitivity studies applied to a two-dimensional resistivity model from the Central Andes: Geophysical Journal International, v. 150, no. 3, p. 673-686.

Schwalenberg, K., Rippe, D., Koch, S., and Scholl, C., 2017, Marine-controlled source electromagnetic study of methane seeps and gas hydrates at Opouawe Bank, Hikurangi Margin, New Zealand: Journal of Geophysical Research: Solid Earth, v. 122, no. 5, p. 3334-3350.

Smirnova, M. V., Becken, M., Nittinger, C., Yogeshwar, P., Mörbe, W., Rochlitz, R., Steuer, A., Costabel, S., Smirnov, M. Y., and the, D. W. G., 2019, A novel semiairborne frequency-domain controlled-source electromagnetic system: Three-dimensional inversion of semiairborne data from the flight experiment over an ancient mining area near Schleiz, Germany: Geophysics, v. 84, no. 5, p. E281-E292.

Steuer, A., Smirnova, M., Becken, M., Schiffler, M., Günther, T., Rochlitz, R., Yogeshwar, P., Mörbe, W., Siemon, B., Costabel, S., Preugschat, B., Ibs-von Seht, M., Zampa, L. S., and Müller, F., 2020, Comparison of novel semi-airborne electromagnetic data with multi-scale geophysical, petrophysical and geological data from Schleiz, Germany: Journal of Applied Geophysics, v. 182.

Strack, K. M., 1992, Exploration with Deep Transient Electromagnetics, Elsevier.

Vozoff, K., and Jupp, D. L. B., 1975, Joint Inversion of Geophysical Data: Geophysical Journal International, v. 42, no. 3, p. 977-991.

Wagner, F. M., Mollaret, C., Günther, T., Kemna, A., and Hauck, C., 2019, Quantitative imaging of water, ice and air in permafrost systems through petrophysical joint inversion of seismic refraction and electrical resistivity data: Geophysical Journal International, v. 219, no. 3, p. 1866-1875.

Wang, S., Bastani, M., Constable, S., Kalscheuer, T., and Malehmir, A., 2019, Boat-towed radio-magnetotelluric and controlled source audio-magnetotelluric study to resolve fracture zones at Äspö Hard Rock Laboratory site, Sweden: Geophysical Journal International, v. 218, no. 2, p. 1008-1031.

6 Appendix

6.1 1D resolution study

The resolution capability was compared for the magnetic field transfer function from semi-AEM data and the electric field from LOTEM data via a synthetic study. The 1-D resistivity model depicted in Figure A 1a is an approximate simulation for the target conductor in the survey area. In Figure A 1b to e, the misfit spaces (with $\chi < 2.0$) for the true model (Figure A 1a) as a function of perturbations to resistivity and thickness of target layer are plotted for LOTEM and semi-AEM data. The used frequency and time ranges are the same as those in Table 1. Both typical Gaussian noise of LOTEM (2%) and semi-AEM (5%) were tested. The parameters values of the true model are highlighted as blue plus signs. For both methods, the ratio between resistivity and thickness of the target layer is similar among the models with low misfits. However, the misfit spaces between the two methods are differently distributed. The low misfit regions of the LOTEM cases are longer and thinner than those of the semi-AEM data, indicating the distinct resolution. Given the same transmitter and offsets, the observed resolution distinctions are led by the different EM components in each typical frequency or time range.

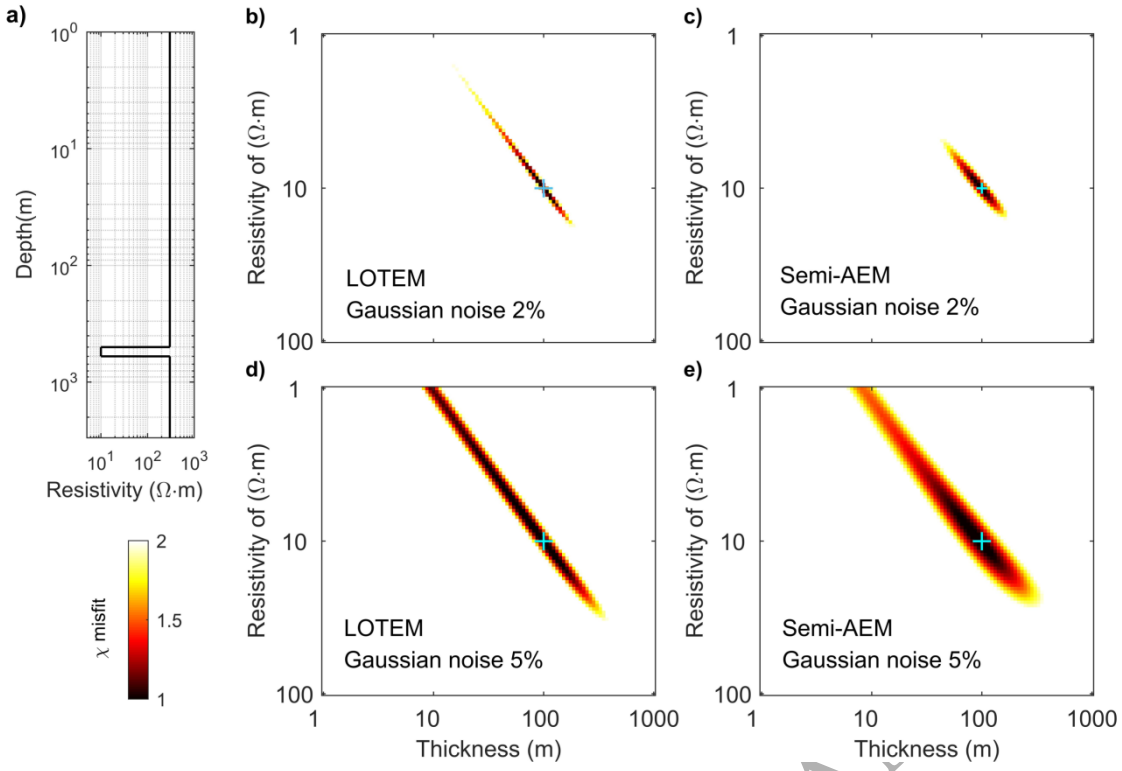

Figure A 1. Resolution studies for the typical semi-AEM Bz transfer function and LOTEM Ex step-on transient in 1-D case. (a) Sketch of a 1-D resistivity model. The modelling studies investigating the resolution of LOTEM and semi-AEM data to the resistivity and thickness of the target conductive layer in (a) are shown in (b) and (c) for a 2% Gaussian noise, and (d) and (e) for a 5% Gaussian noise. The transmitter length is 1000 m and the current is 1 A. The offset is 1500 m for both LOTEM and semi-AEM measurements. The altitude of semi-AEM receivers is 40m.

6.2 2-D effects in the 1-D joint inversion

The 2-D effects in the 1-D joint inversions were investigated. We considered a simple 2-D resistivity model shown in Figure A 2, which has only one 2-D boundary at offset 1100m. 1-D Occam inversions were applied to the semi-AEM and LOTEM synthetic data of this 2-D model individually (Figure A 2 a and b) and jointly (Figure A 2 c). When the 2-D effects are relatively weak (e.g., at an offset of 700 m), both individual method

inversions and the joint inversion can resolve the target layer. When the 2-D effects are strong (e.g., at an offset larger than 1100 m), the 2-D effects lead the individual method inversions to converge in different directions, generating different models (which can be explained by the individual datasets); for joint inversion, the distinct model updates needed for the two datasets lead to poor convergence rates, and no common model can be found finally.

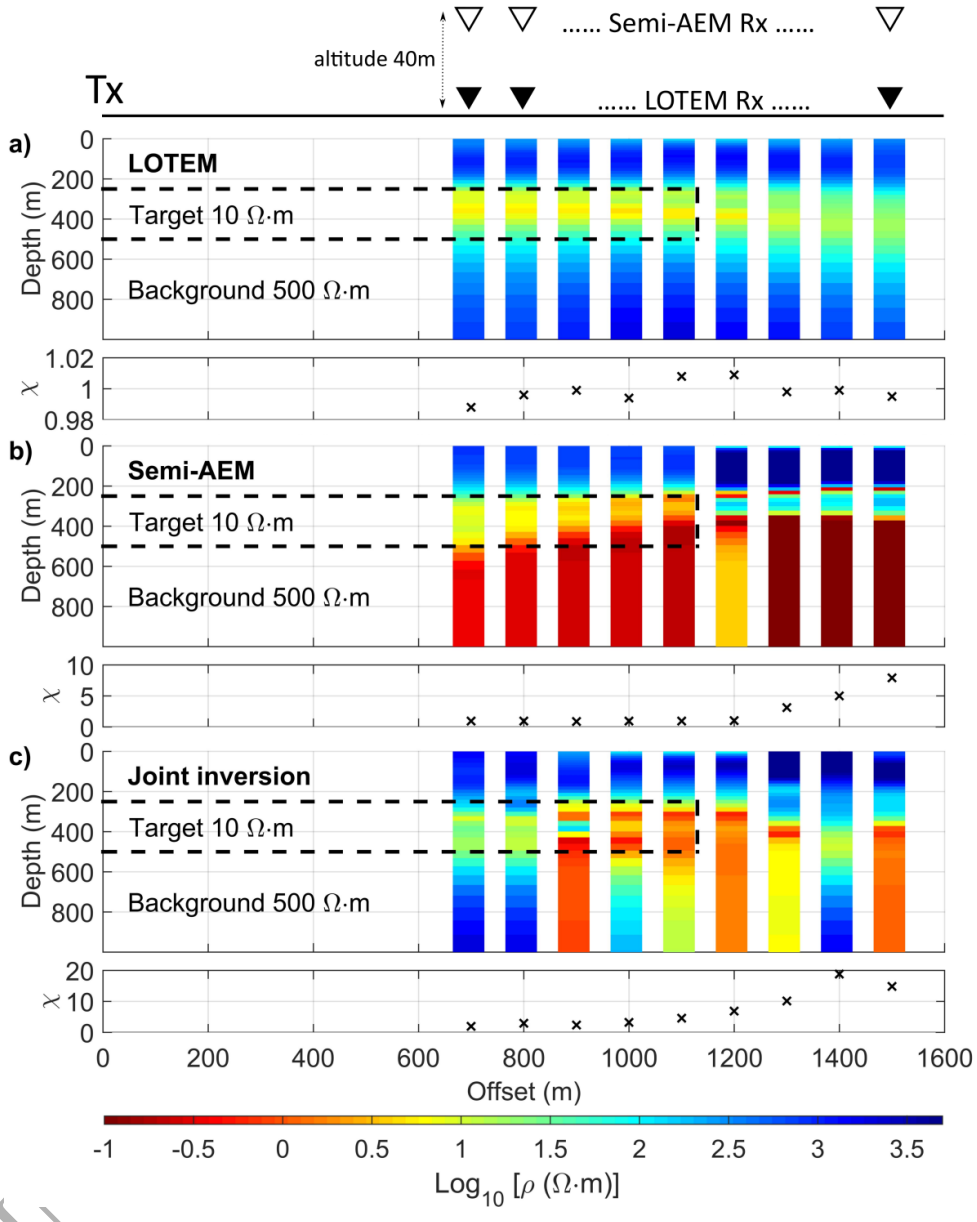

Figure A 2. 1-D Occam inversion results for 2-D synthetic data. (a) LOTEM; (b) Semi-AEM; (c) Joint inversion. The data misfits are displayed for each station. The altitude of semi-AEM receivers is 40m. A point source is considered. A 1-D Occam algorithm is used with the roughness-1 proposed by (Constable et al., 1987).